Lou, Siwei et al.

Article

Solar energy and daylight on tilt planes under CIE standard skies

Energy Reports

Provided in Cooperation with:
Elsevier

Suggested Citation: Lou, Siwei et al. (2020) : Solar energy and daylight on tilt planes under CIE standard skies, Energy Reports, ISSN 2352-4847, Elsevier, Amsterdam, Vol. 6, pp. 895-905, https://doi.org/10.1016/j.egyr.2020.04.014

This Version is available at:
https://hdl.handle.net/10419/244087

Energy Reports 6 (2020) 895–905

Contents lists available at ScienceDirect

Energy Reports

journal homepage: www.elsevier.com/locate/egyr

Research paper

Solar energy and daylight on tilt planes under CIE standard skies

Siwei Lou [a], Danny H.W. Li [b], Dawei Xia [c,*], Isaac Y.F. Lun [d], Wenqiang Chen [b], Yanping Yang [a]

[a] School of Civil Engineering, Guangzhou University, 230 Guangzhou Higher Education Mega Centre West Outer Ring Road, Panyu District, Guangzhou, China
[b] Building Energy Research Group, Department of Architecture and Civil Engineering, City University of Hong Kong, Tat Chee Avenue, Kowloon, Hong Kong, China
[c] School of Architecture and Urban Planning, Guangzhou University, 230 Guangzhou Higher Education Mega Centre West Outer Ring Road, Panyu District, Guangzhou, China
[d] Department of Architecture and Built Environment, University of Nottingham Ningbo China, 315100, China

ARTICLE INFO

Article history:
Received 23 October 2019
Received in revised form 5 April 2020
Accepted 5 April 2020
Available online xxxx

Keywords:
CIE Standard Skies
Sky diffuse
Anisotropic sky
Inclined sky component
Surrogate model

ABSTRACT

The CIE (International Commission on Illuminance) Standard Skies depicts the typical diffuse luminance and radiance distributions over the skydome. However, it can be challenging to interpret the luminance and radiance distribution into the irradiance and illuminance contributions on tilt planes by numerical integrations. This paper proposes a surrogate model that determines the ratio of the diffuse irradiance on an arbitrary tilt plane to that on the unobstructed horizontal plane without the complicated and time-consuming numerical integrations. The model is determined using solar altitude, sky conditions, and the angular distance of the plane (surface normal) and the sun. The proposed model is validated by measurement of the vertical illuminance and irradiance that are taken in 2004 and 2005, and the irradiance on planes of different tilt angles and azimuth directions from February to May in 2015. All measurements were in the 10-minute interval. For vertical planes, the proposed approach gives the ratio of the root mean square errors to the measurement average 1.38% to 2.04% lower than a classical model for irradiance and 3.6% to 4.6% for illuminance, when the Skies can be accurately identified. The model thus accurately interprets the luminance and radiance distributions of the CIE Standard Skies, which can be essential to a fast study for the solar energy potential as well as the thermal and daylight environments under different sky conditions.

1. Introduction

Solar radiation and daylight data are essential to the architects and engineers for energy saving and the designs of visual comfort and green building (Costanzo et al., 2018; Li et al., 2019b; Sudan and Tiwari, 2016). The solar energy on a building envelope may impose significant heat gain, while, on the other hand, this same energy can be harvested by photovoltaic (PV) panels (Luo et al., 2018). Recently, many PV panels were installed at high tilt angles or even vertically on building facades for more energy gain (Ghazali et al., 2017; Lee et al., 2017). The placements are different from the conventional horizontal installations, and it is essential to estimate the solar irradiance on PV panels of different tilt angles (Ben Othman et al., 2018). The daylighting has been proven to be effective in saving the artificial lighting energy and reducing its cooling load (Chi et al., 2018; Shishegar and Boubekri, 2017). The solar radiation and daylight data on or through the vertical and tilted building envelop are thus important to the low energy building studies (Lou et al., 2016). Conventionally, the irradiance (W/m^2) and illuminance (lux) data are usually measured on horizontal planes as the routine task of weather stations or research institutes (Fan et al., 2019). However, there is a high demand for models that can accurately estimate the data in arbitrary directions using historical data records.

The solar radiation and daylight consist of the direct and diffuse components (Lou et al., 2016; Tian et al., 2018). The direct part is from the sun, and transfers in a single direction that is defined by the solar altitude and azimuth angles. The diffuse part is from the sky that varies in different directions, which can be affected by the sun position, the ground, and the weather (Li et al., 2019a; Lou et al., 2019b, 2017). The early-stage studies assumed uniform (Liu and Jordan, 1963) or azimuthal homogeneous (Moon and Spencer, 1942) sky radiance (W/(m^2

* Corresponding author.
E-mail addresses: swlou2-c@my.cityu.edu.hk (S. Lou), bcdanny@cityu.edu.hk (D.H.W. Li), xiadawei@gzhu.edu.cn (D. Xia), Isaac.Lun@nottingham.edu.cn (I.Y.F. Lun), wenqichen6-c@my.cityu.edu.hk (W. Chen), 1402061719@qq.com, yypzzm@gzhu.edu.cn (Y. Yang).

https://doi.org/10.1016/j.egyr.2020.04.014

Nomenclature

E	Full-spectrum irradiance W/m^2
I	Visible illuminance lux
R	Sky radiance or luminance W/(m^2 sr) or lux/sr
R_Z	Sky radiance or luminance of the sky zenith point
$R_{\alpha\phi}$	Sky radiance or luminance of the sky element in α and ϕ
R^2	Coefficient of determination, percentage of the output variations that can be determined by the model
Z	Zenith angle of an arbitrary sky element
Z_S	Zenith angle of the sun
r_g	The reflectance of the ground
x	The input variable of the artificial neural network
z	The output of the hidden neural of the artificial neural network

Abbreviations

ANN	Artificial neural network
CIE	International Commission of Illumination
CTree	Classification algorithm or model
ISC	Inclined sky component, the ratio of the diffuse irradiance (or illuminance) on inclined planes to that on horizontal planes under the same sky radiance (or luminance) distribution
RMSE	Root mean square error
VSC	Vertical sky component, the ratio of the diffuse irradiance (or illuminance) on vertical planes to that on horizontal planes under the same sky radiance (or luminance) distribution
%RMSE	The ratio of RMSE to the measurement average

Greek letters

α	Altitude angle of an arbitrary sky element
β	The tilt angle of the plane under consideration
ϕ	The azimuth angle of an arbitrary sky element
ϕ_S	The azimuth angle of the sun
ϕ_N	The azimuth angle of the plane direction
χ	Scattering angle, the angular of an arbitrary sky element to the sun
χ_{ref}	Reference scattering angle, the angle of the sky element in the ϕ_N direction to the sun
σ	The incidence angle of an arbitrary sky element to the plane under consideration
σ_S	The incidence angle of the sun to the plane under consideration

Subscripts for *E* and *I*

B	The direct beam (irradiance or illuminance) on the ground level
D	The diffuse (irradiance or illuminance) on the ground level
G	The global (irradiance or illuminance) on the ground level
H	(irradiance or illuminance) on a horizontal plane, as the first subscript of E and I
N	(irradiance or illuminance) in the transferring direction of the sunlight
V	(irradiance or illuminance) on a vertical plane, as the first subscript of E and I
β	(irradiance or illuminance) on a plane tilt by an angle of β, as the first subscript of E and I

sr)) and luminance (cd/m^2, i.e., lux/sr) distributions. This assumption, for simplicity, represents the overcast sky conditions that are usually regarded as the worst condition for daylighting. As a result, the daylight factor (Bournas and Dubois, 2019; Sudan et al., 2015) can be straightforward to indicate the daylight accessibility in different parts of the room according to the plan and fenestration layouts. However, the azimuthal homogeneity assumption was not accurate nor flexible enough for the daylight illuminance and solar irradiance estimations with the changing solar position (Mangione et al., 2018; Tregenza, 1980). Recently, the International Commission of Illumination (CIE) adopted 15 standard sky models that give the relative brightness of the sky luminance in any sky directions and conditions from overcast to partly cloudy and clear (CIE/ISO, 2003; Kittler and Darula, 2016). Though the Sky model was developed for daylight, it has been appropriately used in solving the full-spectrum radiation problems (i.e., the radiance distribution = luminance distribution). An underlying assumption is that the luminance efficacy is identical in sky directions of different azimuth and altitude angles, which is supported by works on diffuse luminance efficacy (Robledo and Soler, 2001, 2003), and has been successfully used in studies on the vertical radiation (Alshaibani, 2011; Li et al., 2011). The CIE Standard Sky model has been proven to represent the worldwide sky conditions well (Lou et al., 2019b; Suárez-García et al., 2018), and can estimate the illuminance accurately (Kim and Kim, 2019; Yun and Kim, 2018).

However, the CIE Standard Skies determine the luminance (or radiance) distribution only, and the irradiance (W/m^2) and illuminance (lux) on a tilted plane should be determined by numerical integrations (Tregenza and Waters, 1983). The numerical integration can be difficult and time-consuming, because some sky elements can be obstructed, and the others can be of various incident angles on the plane of interest. In addition, the CIE standard sky models depict the ratio of the luminance or radiance in a sky direction to the zenith, yet the zenith data are not commonly measured. In this connection, it is expected that the interpretation of luminance and radiance distributions to the radiation and lux levels could be simplified. The zenith term can be cancelled out by the ratio of the diffuse irradiance and illuminance on the vertical (and tilt) plane to that on the unobstructed horizontal plane (Chen et al., 2019; Li et al., 2011). The ratios were named as the Vertical and Inclined Sky Components (VSC and ISC), which was determined according to the solar angles with respect to the facing directions of the plane. The indices are

essential to calculating the solar irradiance on tilt planes when the sky conditions are known (Li et al., 2013), or identifying the sky conditions if the irradiance on vertical planes is measured (Li et al., 2014). Previously, we determined the ISC indices for planes of several specific tilt angles (Li et al., 2016) only, while the model was not generalized for planes of arbitrary tilt angles for universal studies. Besides, the solar altitude angle (α_S) that affects the VSC values were overlooked as noises (Li et al., 2015) for simple curve fittings, which, however, leads to uncertainties of the outcome accuracies.

As the further work of Li et al. (2016), this work develops an updated model that gives the VSC and ISC values of planes in an arbitrary tilt angle (including 90°, i.e. vertical) under the 15 CIE standard skies. Additionally, α_S is considered in the model as a factor that affects the VSC and ISC values. Firstly, the diffuse solar radiation and daylight on horizontal and inclined planes of different tilt angles are integrated by numerical integrations for accurate VSC and ISC values. The integration results are then correlated to the factors including the solar and plane angles, and the CIE standard sky type by the artificial neural network (ANN). Here, the ANN replaces the numerical integration as a surrogate model, which is different from the black-box data-driven models (Dahmani et al., 2014; Notton et al., 2012) that avoid specifying the sky anisotropic radiance/luminance features. The ISC and VSC of Skies 1, 3 and 5 are determined by plane tilt angle only, and the correlations are expressed as simple equations. The resulting outcome diffuse irradiance and illuminance are validated by the measurements in different tilt angles and azimuthal directions. The findings and implications are discussed.

2. Methodology

The global irradiance and illuminance ($E_{\beta G}$) on an unobstructed tilt plane (by β (rad)) consist of the direct ($E_{\beta B}$), diffuse ($E_{\beta D}$) and the ground reflected ($E_{\beta R}$) components, as given by Eq. (1). The direct component is from the solar disc and can be determined by Eq. (2). The reflected component can be assumed isotropic for engineering purposes and is given as Eq. (3). In the equations, σ_S is the incidence angle of the direct sun that can be determined by Eq. (4). ϕ_S and ϕ_N are the azimuth angles of the sun and the plane, respectively. r_g is the reflectance of the ground. E_{NB} represents the beam irradiance or illuminance in the direction of the sun, and E_{HG} is the global irradiance or illuminance on the horizontal plane. E_{NB} and E_{HG} are usually accessible by the routine measurements of typical weather stations. E_{NB} may not be measured for some places, yet it can be estimated according to E_{HG} and the solar altitude angle α_S. Without measurements, the illuminance can be determined by irradiance referring to extraterrestrial luminance efficacy of 97.6 to 98.2 lm/W (Darula et al., 2005), or via specific models that have been reviewed in reference (Li and Lou, 2018).

$$E_{\beta G} = E_{\beta R} + E_{\beta B} + E_{\beta D} \tag{1}$$

$$E_{\beta B} = E_{NB} \cos \sigma_S \tag{2}$$

$$E_{\beta R} = r_g E_{HG} \left(1 - \cos \beta\right)/2 \tag{3}$$

$$\cos \sigma_S = \sin \alpha_S \cos \beta + \cos \alpha_S \sin \beta \cos \left(\phi_S - \phi_N\right) \tag{4}$$

The diffuse irradiance (and illuminance) is determined by the sky radiance (and luminance) that can be different in all the sky directions. For a tilted plane, a particular part of the sky is obstructed (by the plane itself), making no contribution to the irradiance (and illuminance) on the plane. In this connection, the contribution of the sky directions to the plane should be considered direction-by-direction. The irradiance and illuminance contributions of an infinitely small sky patch can be determined by Eq. (5). $R_{\alpha\phi}$ is the radiance and luminance of the sky element in an altitude α and an azimuth ϕ. The second and third terms in the brackets are the incidence angle, and the solid angle of the sky element, respectively.

$$\delta E_{\beta D} = R_{\alpha\phi} \left(\cos \beta \sin \alpha + \sin \beta \cos \alpha \cos \phi\right) \left(\cos \alpha \delta\alpha \delta\phi\right) \tag{5}$$

Eq. (5) should be double integrated over the ranges of the sky altitude α and azimuth ϕ angles as given in Eq. (6). The lower and upper limits of α should be 0 and $\pi/2$, respectively. For β lower than $\pi/2$ (90°), the limits of ϕ should be $\phi_N \pm \pi$, and the lower and upper limits of α should be α_P and $\pi/2$, respectively. α_P can be determined by ϕ according to Eq. (7). For $\beta = \pi/2$ (vertical planes), the upper and lower limits of ϕ should be $\phi_N \pm \pi/2$.

$$\delta E_{\beta D} = \iint R_{\alpha\phi} \left(\cos \beta \sin \alpha \cos \alpha + \sin \beta \cos 2\alpha \cos \phi\right) \delta\alpha \delta\phi \tag{6}$$

$$\alpha_P = \max \left\{0, \tan^{-1} \left[\frac{-\cos \left(\phi_N - \phi\right)}{\cot \beta}\right]\right\} \tag{7}$$

2.1. The radiance and luminance distributions of the CIE standard skies

The 15 CIE Standard Sky models depict the ratio between the radiance and luminance at an arbitrary sky point ($R_{\alpha\phi}$) to that at sky zenith (R_Z) by Eq. (8). The CIE Skies were initially proposed for daylight luminance, yet have been used in many radiance studies with good performances. The equation is the product of the relative gradation $\varphi(Z)/\varphi(0)$ and indicatrix functions $f(\chi)/f(Z_S)$. Z is the zenith angle of the sky point under evaluation, $Z = \pi/2 - \alpha$; Z_S is the zenith angle of the sun; a, b, c, d, and e are coefficients, and their values can be adjusted to depict the 15 CIE standard sky conditions from heavily overcast to clear. Eq. (9) gives the scattering angle χ (rad) that describes the shortest angular distance between the sky element and the solar disc; and ϕ_s in Eq. (9) is the azimuth angle of the sun.

The CIE Standard Skies can be determined by several approaches. The most comprehensive approach is to measure the luminance of many (145 in the current study) sky directions. The 15 theoretical CIE Standard Sky models should be compared to the luminance measurements, which selects the model that best described the reality (Tregenza, 2004). Fig. 1 gives the general features of the 15 CIE standard skies, and their occurrence frequency according to our previous studies by the sky scanner EKO-301LR from 2004 to 2005 (Lou et al., 2019b). For simplicity, the radiance distribution was determined by the luminance with the underlying assumption of the same luminance efficacy in all the sky directions. The figure describes high occurrences of overcast sky 1, partly cloudy sky 8, and clear sky 13 for the local subtropical climate, which is similar to the other local (Ng et al., 2007), and overseas studies in the tropical climate (Witkopf and Soon, 2007). Additionally, we developed an empirical Classification Tree that estimates the overcast, partly cloudy and clear skies using the horizontal global irradiance and illuminance data (Lou et al., 2017). These variables should be more readily accessible than luminance distribution that is difficult to measure in the long run. The sky conditions of 2015, for the validation of the tilt planes, were estimated by this approach only, since the luminance distributions were not measured then.

$$\frac{R_{\alpha\varphi}}{R_Z} = \frac{\phi\left(Z\right) f\left(\chi\right)}{\phi\left(0\right) f\left(Z_S\right)} = \frac{1 + a \exp\left(b/\cos Z\right)}{1 + a \exp b} \times \frac{1 + c\left[\exp\left(d\chi\right) - \exp\left(d\pi/2\right)\right] + e \cos 2\chi}{1 + c\left[\exp\left(dZ_S\right) - \exp\left(d\pi/2\right)\right] + e \cos 2Z_S} \tag{8}$$

$$\chi = \arccos\left(\cos Z_S \cdot \cos Z + \sin Z_S \cdot \sin Z \cdot \cos\left|\varphi - \varphi_S\right|\right) \tag{9}$$

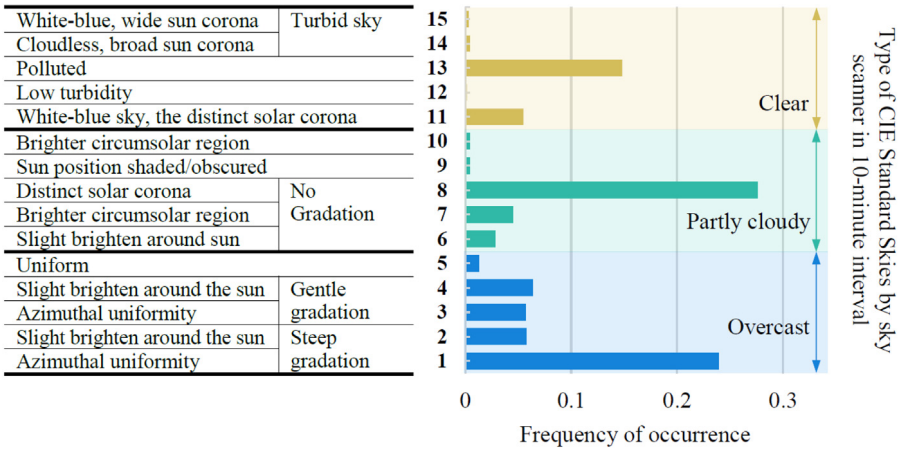

Fig. 1. The occurrence frequency of ISO/CIE Standard Skies of Hong Kong, based on the data from 2004 to 2005 (Lou et al., 2019b).

Table 1
Minimum and maximum of the ANN inputs and output for ISC.

Coefficients	c_1	c_2	c_3	c_4
Sky 1	1.074	−0.01872	1.711	−0.0733
Sky 3	1.161	−0.008727	1.962	−0.1602
Sky 5	1.383	0.002739	2.339	−0.3827

2.2. Inclined sky component by the surrogate model

It can be challenging to integrate the radiance and luminance distributions over the sky altitude and azimuth angles analytically. The numerical integrations were possible, while the architects and engineers may not be fully familiar with it. Additionally, the outcomes can be related to the zenith radiance or luminance that are not available from the measurements of common weather stations. In this connection, the inclined sky component (ISC) is defined to cancel out the zenith values, and for engineering uses. The ISC is the ratio of the diffuse irradiance or illuminance on the plane tilt by β to that on the unobstructed horizontal plane ($E_{\beta D}/E_{HD}$).

Fig. 2 gives the ISC values of the planes tilted by 0 to $\pi/2$ under CIE standard Skies 1, 3, and 5 that are determined by numerical integrations. The ISCs of Skies 1, 3, and 5 were determined by the tilt angle β only because the radiance distributions are homogeneous in all azimuthal directions. The ISC was around 1 for β lower than $\pi/12$ (15°), indicating the horizontal and tilt irradiance and illuminance were similar for planes of low β. Then the ISC reduced gradually for β lower than $\pi/4$ (45°), yet it was still higher than 0.79. Finally, the ISC reduced notably to around 0.35 to 0.41 when β increased from $\pi/4$ (45°) to $\pi/2$ (90°), indicating the $E_{\beta D}$ can be greatly lower than the E_{HD} due to a high tilt angle β. ISC of Sky 1 reduced more significantly compared to the uniform sky 5, which is because the low latitude sky regions were darker than the sky zenith. The sky elements around the horizon were around one-third of that on the sky zenith for Sky 1, and the maximum ISC difference between Skies 1 and 5 for $\beta = \pi/2$ was around 0.12. In this connection, $E_{\beta D}$ on vertical planes tends to be lower than half of E_{HD} under the overcast skies, considering the Sky 1 tends to be the frequent overcast sky in many places of the world (Luo et al., 2014; Ng et al., 2007; Suárez-García et al., 2018; Tregenza, 2004; Wittkopf and Soon, 2007). Estimating $E_{\beta D}$ by a uniform assumption leads to a maximum error as high as 0.12/0.379 = 31.7% for vertical planes in overcast conditions. The curves in Fig. 2 can be approximated by Eq. (10) ($R^2 = 1$), where the coefficients are given by Table 1.

$$\mathrm{ISC} = c_1 \exp\left\{-\left[(x - c_2)/c_3\right]^2\right\} + c_4 \tag{10}$$

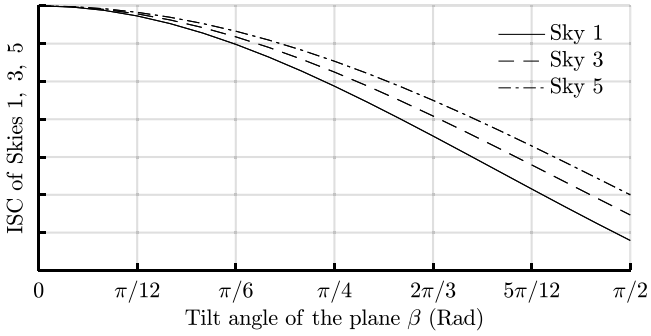

Fig. 2. ISC of planes tilt by 0 to $\pi/2$ under CIE standard Skies 1, 3 and 5.

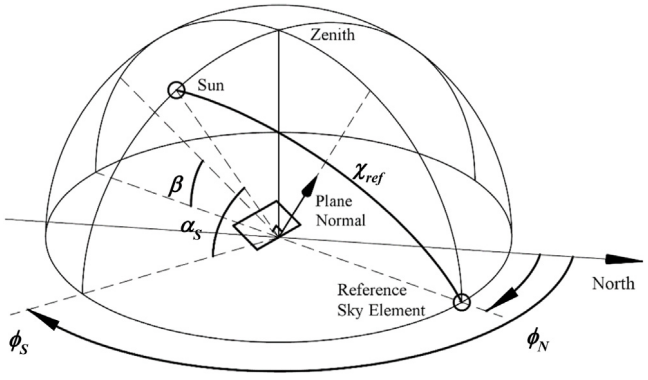

Fig. 3. Angles defining the position of the sun and a reference sky element.

For skies with circumsolar brightening, the ISC should be determined by the solar position referring to the plane, and the solar altitude angle as well as β. The reference scattering angle (χ_{ref}) is defined to describe the solar position with respect to the plane. χ_{ref} is the shortest angular distance between the solar disc and the sky element with the azimuth angle of the plane ϕ_N at zero altitudes, as given in Fig. 3. The ISC values of Sky 8 for planes with tilt angles of $\pi/2$ (90°), $\pi/4$ (45°), and $\pi/6$ (30°) are given in Fig. 4. Sky 8 was the most frequent one in Hong Kong given by the 2004 and 2005 measurements in Fig. 1. For all β and α_S, the ISC values peaked at χ_{ref} lower than $\pi/6$ and reduced to their minimums at χ_{ref} higher than $\pi/2$. This shows the ISC was highest for the sun-facing planes, and $E_{\beta D}$ can be higher than E_{HD} for the cases of low χ_{ref} and low β angles. In addition, the figure indicates that, for Sky 8, the ISC of planes with low β was, in general, higher than those

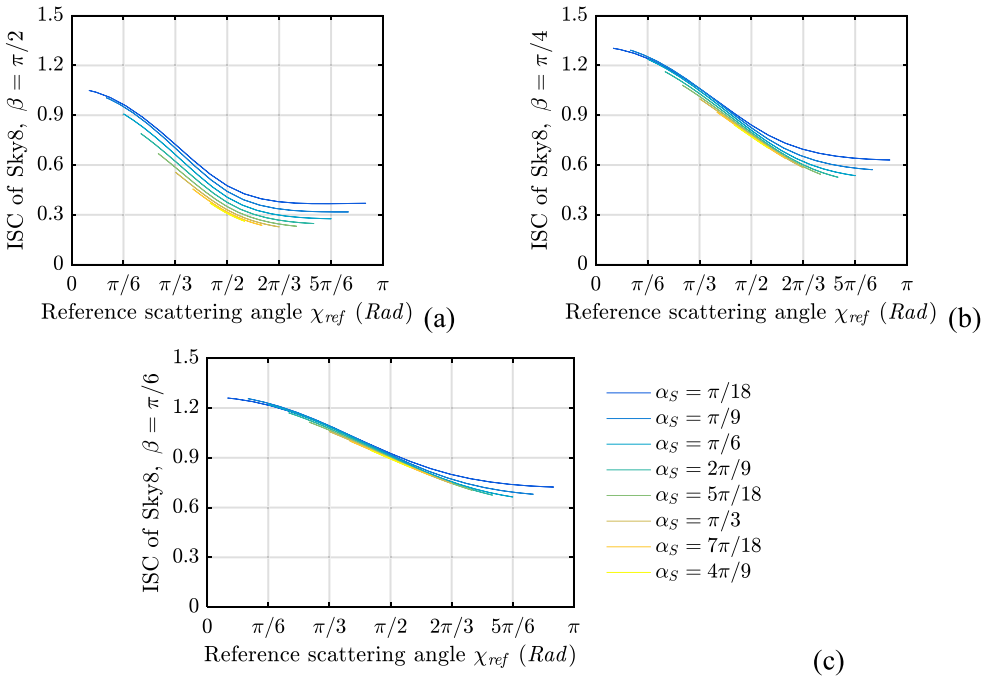

Fig. 4. The ISC of CIE partly cloudy Sky 8 for planes of different tilt angles.

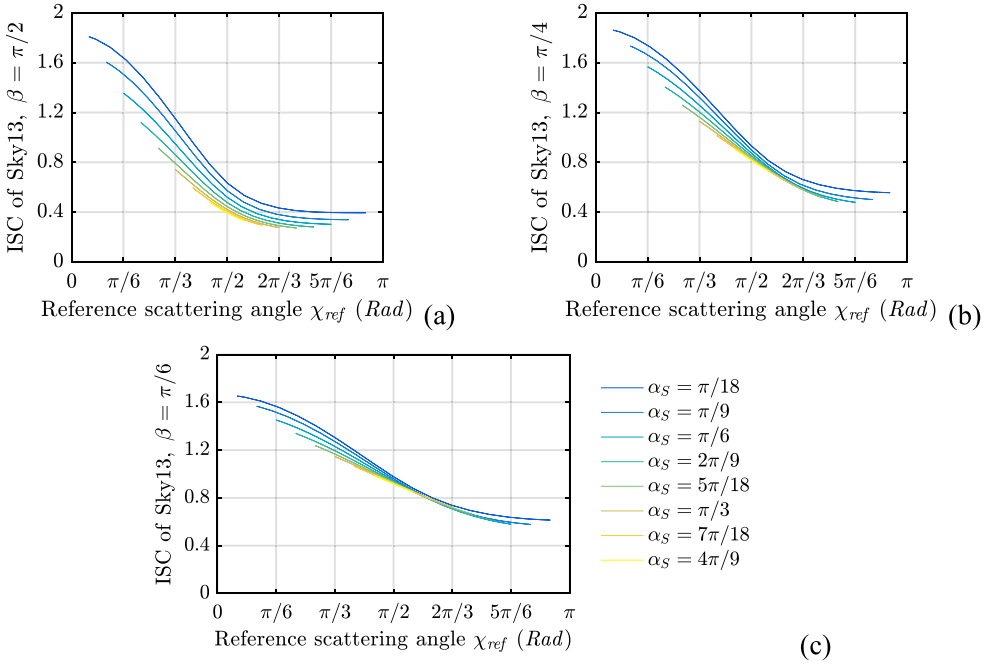

Fig. 5. The ISC of CIE clear Sky 13 for planes of different tilt angles.

with a high β, regardless of the scattering angles. The peak ISC, however, was around 1.05, 1.3 and 1.26 for planes tilt by $\pi/2$, $\pi/4$, and $\pi/6$, respectively. This indicates that the peak ISC levelled off when β increased from $\pi/6$ to $\pi/4$ yet reduced slightly for β increased further. For the sun-shaded planes with χ_{ref} higher than $\pi/2$, on the other hand, the ISC can be lower than 1, indicating the $E_{\beta D}$ is lower than E_{HD}. The minimum ISC was around 0.227 to 0.367 for vertical planes, which was comparable to the overcast Sky 1. This indicates the sun-shaded planes under partly cloudy skies can access less daylight and radiation than the overcast skies that were regarded as the literately worst condition. The solar altitude, in addition, leads to uncertainties of the ISC for a given χ_{ref} and β, especially for the vertical planes. For vertical planes with $\chi_{ref} = 2\pi/3$ (60°), for example, the ISC of $\alpha_S = \pi/9$ was 0.111 higher than that of $\alpha_S = \pi/3$, and the difference accounted for 36% of the case with $\alpha_S = \pi/3$ (ISC = 0.31). In this connection, the ISC of the 15 CIE standard skies should be determined by α_S, χ_{ref}, and β.

Fig. 5 illustrates the ISC of Sky 13 for planes tilt by $\pi/2$, $\pi/4$ and $\pi/6$, and this represents the most frequent clear sky given by the data of Hong Kong from 2004 to 2005 in Fig. 1. For Sky 13, the trends of ISC curves for different χ_{ref} values were similar to that of Sky 8 given in Fig. 4. The ISC of $\chi_{ref} < \pi/2$ under the clear Sky 13 increased consistently when β increased from $\pi/6$

Table 2
Minimum and maximum of the ANN inputs and output for ISC.

Variables	x_1 (Sky type)	x_2 (χ_{ref})	x_3 (α_S)	x_3 (β)	ISC
Minimum	2	0	0	0	0.2274
Maximum	15	π	$\pi/2$	$\pi/2$	2.7071

to $\pi/2$. The peak ISC values of different tilt angles, however, were similar for all cases under evaluation, which were higher than 1.6, and the corresponding χ_{ref} were lower than $\pi/6$. This value was higher than the partly cloudy Sky 8, because of the more distinct sun corona of the clear sky compared to the partly cloudy one. This explains the more significant differences of the ISC values of the sun-facing (e.g., $\chi_{ref} < \pi/6$) against the sun-shaded cases (e.g., $\chi_{ref} > 5\pi/6$ (150°)) for Sky 13 compared to that of the partly cloudy Sky 8 in Fig. 4. For planes tilt by $\pi/2$ under Sky 13, the ISC uncertainties due to α_S were significant for the sun-facing cases when χ_{ref} was less than $\pi/2$. For vertical planes ($\beta = \pi/2$), the ISC of $\alpha_S = \pi/3$ was 0.72 at $\chi_{ref} = \pi/3$, which was 0.3 lower than that of $\alpha_S = \pi/9$ (20°). The ISC uncertainty due to α_S, however, was less significant for planes tilt by $\pi/4$ or less, especially for the sun-shaded cases with $\chi_{ref} < \pi/2$. Similar trends of the ISC at different χ_{ref} were found for the other CIE Sky conditions.

2.3. Surrogate model for the numerical integration

The findings of the numerical integration, as presented in the last section, indicate that the ISC can be determined by χ_{ref}, β, and α_S. However, the integration can be difficult, and it is thus expected to develop a surrogate model for fast calculations to solve engineering problems. Previously, the uncertainties of ISC due to α_S were regarded as noises, and the ISC of different α_S values were smoothed by χ_{ref}, which may lead to errors, especially for vertical planes as given in Figs. 4(a) and 5(a). In this connection, the artificial neural network (ANN) was used as a surrogate model of numerical integration, which correlated the ISC with the variables χ_{ref}, β, and α_S. The ANN was developed according to the results of ISC that is numerically integrated by the 'integral2' function of MATLAB. β and α_S were set as 0, $\pi/36$ (5°), $\pi/18$ (10°), ..., $\pi/2$ (90°), and ϕ_S was set as 0, $\pi/18$ (10°), $\pi/9$ (10°), ..., 2π (360°) for the CIE standard Skies excluding Skies 1, 3 and 5, which gives 160,284 sets of integration outcomes for the ANN correlations. The Skies 1, 3 and 5 were excluded because their ISC was determined by β only.

The neural network consisted of the input, hidden and output layers, as given in Fig. 6. The input variables should be mapped to the range from −1 to 1 by Eq. (11). Similarly, the output of the ANN ranges from −1 to 1, and should be converted to the ISC values by Eq. (12). $x_{j,real}$ is the value of the jth input variable, and $x_{j,max,}$ and $x_{j,min}$ are the maximum and minimum values of it. Similarly, $\mathrm{ISC_{max}}$ and $\mathrm{ISC_{min}}$ are the maximum and minimum of the ISC values. x_j and y are the normalized jth input and output variables, respectively. Table 2 gives the maximum and minimum values of the input and output variables. The calculations of the hidden and output layers are given by Eqs. (13) and (14), respectively. $w_{i,j}$ and b_i are the weight of variable x_j and the bias of the ith hidden neuron in the hidden layer. w_i' and b' are the weight and bias of the ith hidden neuron output in the output layer, respectively.

$$x_j = 2\left(x_{j,real} - x_{j,\min}\right)/\left(x_{j,\max} - x_{j,\min}\right) - 1 \tag{11}$$

$$\mathrm{ISC} = 0.5\,[y+1]\,(\mathrm{ISC_{max}} - \mathrm{ISC_{min}}) + \mathrm{ISC_{min}} \tag{12}$$

$$z_i = 2\Bigg/\left(1 + \exp\left[-2\sum_{j=1}^{3}\left(w_{i,j}x_j + b_i\right)\right]\right) - 1 \tag{13}$$

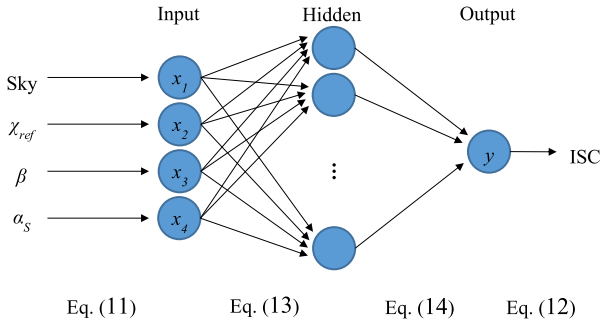

Fig. 6. The Artificial Neural Network of the ISC estimation.

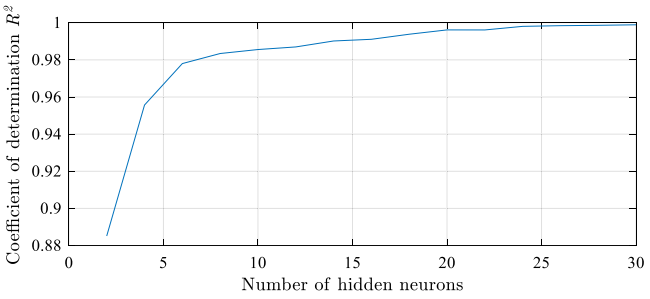

Fig. 7. Coefficient of determination R^2 for ANN with different hidden neurons.

$$y = \sum_{i=1}^{15} w_i' z_i + b' \tag{14}$$

The neural network was trained by the Leverberg–Marquardt optimization of the MATLAB ANN toolbox. Though the algorithm was well-developed, the number of hidden neurons should be determined case by case. The datasets were divided into eight subgroups according to the tilt angle, which gives eight independent ANN training processes to evaluating the performance of the developed ANN on planes of a new tilt angle. Every time, the datasets of two tilt angles were excluded in the training process for each subgroup and were used for testing only. Finally, the estimated testing datasets are combined for the coefficient of determination (R^2) by different hidden neurons. Eq. (15) in Box I gives the math expression of R^2. For every training, the ANN will be developed by 70% of the data and validated by 30% of the rest. The training stops when the error of the validation data rises for 12 successive iterations. The findings of R^2 for ANN with 2, 4, ..., 30 hidden neurons are given by Fig. 7. The figure shows that the R^2 increased rapidly when the hidden neuron increased from 2 to 6. Then R^2 increased moderately, and then levelled off when 22 or more hidden neurons were used. In this connection, the ANN that estimates ISC was developed by the 22 hidden neurons, and the weights and biases for the finalized ANN, trained by all datasets, are given in Appendix. See the equation given in Box I.

3. Model validation and discussion

The model is validated by two groups of data that were acquired in different periods. The first group was the solar irradiance and daylight illuminance on the vertical planes facing the four cardinal directions from January of 2004 to December of 2005. The second group was the irradiance on tilt planes (30°, 45°, 60°) facing the various azimuthal directions (north 0°, northeast 45°, ..., 315°) from the end of February to the end of May of 2015. In the model, the horizontal global and diffuse irradiance were taken at the same time as the vertical and tilt

$$R^2 = 1 - \frac{\sum_{i=1,2,\ldots}^{N} (\text{SurrogateModel}_i - \text{NumericIntegration}_i)^2}{\sum_{i=1,2,\ldots}^{N} \left(\text{NumericIntegration}_i - \left(\sum_{i=1}^{N} \text{NumericIntegration}_i\right) \Big/ N\right)^2} \tag{15}$$

Box I.

Table 3
Numbers of the accepted measurement samples for the data on vertical planes (2004–05).

Tests		Criteria		Radiation data				Visible light data			
Level 0		$\alpha_S > 0$		51,192				51,192			
Level 1		$\alpha_S > 4°$ $E_{HG} > 20$ W/m^2 or $I_{HG} > 2$ kilo-lux		43,582				45,842			
Level 2	2.1	$0 < E_{HG} < E_{HE}$; $0 < I_{HG} < I^1_{HE}$		42,605				40,208			
	2.2	$0 < E_{HD} < 0.8E_{HE}$; $0 < I_{HD} < 0.8I^1_{HE}$									
	2.3	$0 \le (E_{HG} - E_{HD}) < E_{HE}$; $0 \le (I_{HG} - I_{HD}) < I^1_{HE}$									
	2.4	$E_{HD} < 1.1E_{HG}$; $I_{HD} < 1.1I_{HG}$									
Level 3		Valid sky luminance measurements		39,322				38,163			
		Vertical directions		Vertical irradiance				Vertical illuminance			
				N	E	S	W	N	E	S	W
Level 4		$E_{VG} > 20$ W/m^2 or $I_{VG} > 2$ kilo-lux		35,715	36,028	36,100	36,226	36,503	36,621	36,810	36,849
Level 5		E_{VD} and $I_{VD} > 0$	($r_g = 0.16$)	35,647	35,782	35,890	35,453	36,503	36,604	36,802	36,848
			($r_g = 0.24$)	35,530	35,498	35,704	35,221	36,499	36,568	36,800	36,842
Level 6		System errors	($r_g = 0.16$)	35,639	35,655	35,794	35,361	35,303	34,220	36,475	36,825
			($r_g = 0.24$)	35,522	35,371	35,6211	35,130	35,299	34,199	36,475	36,822

Note 1: The extraterrestrial irradiance and illuminance are determined by solar (and daylight) constant of 1367 W/m^2, and 133,800 lux, respectively.

measurements. All data were in a 10-minute interval, and were recorded on the rooftop of a building in the City University of Hong Kong (22.3N, 114.2E). The irradiance was measured by Kipp & Zonen CM11 thermopile pyranometer of the secondary accuracy level. The illuminance was measured by the silicon lux metre MINOLTA T-10M. For the period from 2004 to 2005, the sky luminance was measured using the EKO MS-301LR sky scanner.

The data quality was evaluated referring to the criteria of a CIE Guide of data measurement (CIE, 1994). It was inevitable that there may be some erroneous data though great care was taken to keep the data in good quality. Table 3 summaries the number of accepted samples in each quality control level. Level 0 shows the quantity of the data when the sun is above the horizon according to the solar altitude α_S. Level 1 removes the data samples if their global horizontal solar irradiance (E_{HG}) and daylight illuminance (I_{HG}) were extremely low, which should not be the focus of many renewable energy studies. The 2000 lux lower limit of daylight was determined by the 20 W/m^2 of radiation using a basic luminance efficacy simplification of 100 lm/W, referring to Darula et al. (2005). Level 2 removes the datasets that were out of their usual ranges according to the extraterrestrial horizontal irradiance (E_{HE}) and illuminance (I_{HE}) and the relationship between horizontal global and diffuse irradiance. The subscript H suggests that the data were measured on horizontal planes, G means global, and D means diffuse. The irradiance samples accepted at Level 2 were about 2400 more than the illuminance measurements. Level 3 rejects the datasets because the sky scanner was not functioning properly, and the CIE Sky type cannot be properly classified by the luminance distributions. Around 3300 radiation and 2000 daylight samples were removed in Level 3. Level 4 excludes the cases when the global illuminance or irradiance on either of the four cardinal directions was too low to be the focus, which excluded around 3100 to 3600 radiation data samples and 1300 to 1700 daylight samples. Level 5 removes the cases with vertical diffuse (E_{VD}) < 0, which is affected by the ground reflectance (r_g). However, r_g was of uncertainty, and was set as 0.12, 0.14, . . . , 0.24 for the performance evaluations that lead to different E_{VD}. The quantities of the accepted data for $r_g = 0.16$ and 0.26 were given as examples, which was similar to each other. Level 6 removes the datasets that were far from the estimation of the classical Perez 1990 model (Perez et al., 1990), which was probably due to the malfunction of the system, and usually extended for one or two days. Finally, there were around 35,500 to 36,800 radiation and daylight datasets on the vertical planes accepted for analysis.

The accuracies of the surrogate model were, firstly, evaluated by estimating the irradiance on vertical planes facing the four cardinal directions. For vertical planes, the part of the visible skydome and the incidence angles of sky elements are most different from the horizontal planes among all tilt angles ranging from 0 to $\pi/2$. The diffuse component on vertical planes, in this connection, should be most difficult to estimate by the horizontal data, and most representative for planes of tilt angles lower than $\pi/2$. The accuracy is determined by R^2 (cf. Eq. (15)), the root mean square error (RMSE) as given by Eq. (16), and the ratio of RMSE to the average of the measurement (%RMSE). R^2 and %RMSE refer the error to the divergence and the average of the measurement, respectively, which has been used in many previous works (Lou et al., 2019a,b; Sudan et al., 2017). Fig. 8 demonstrates the %RMSE of the vertical solar irradiance by different approaches and different r_g settings. The 15 CIE Standard Skies were either determined by the luminance distribution that was measured by the sky scanner (Scan) from 2004 to 2005, or by the empirical Classification Tree (CTree) of our previous work using the readily accessible horizontal global and diffuse only (in 2015). 'Scan' and 'CTree', respectively, represent the sky conditions that are determined by a cost-demanding yet accurate approach, and an approach that demands the least input but is less accurate. The results are compared to the accuracy of the 'Classical' model (Perez et al., 1990) that is used in many engineering simulation tools.

$$\text{RMSE} = \sqrt{\sum_{i=1,2,\ldots}^{N} (\text{Estimate}_i - \text{Measure}_i)^2 \Big/ N} \tag{16}$$

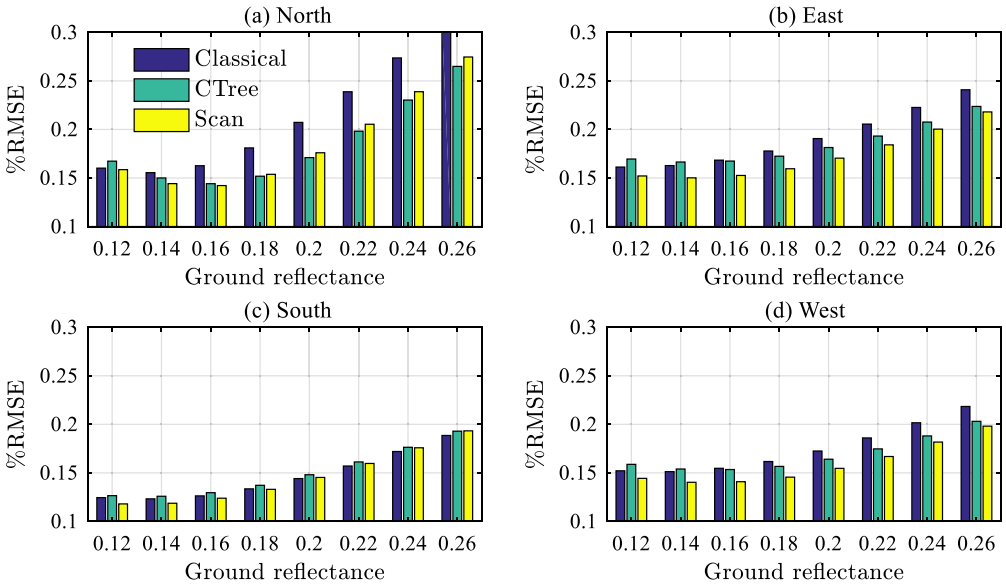

Fig. 8. %RMSE of the global irradiance on vertical planes for different r_g settings.

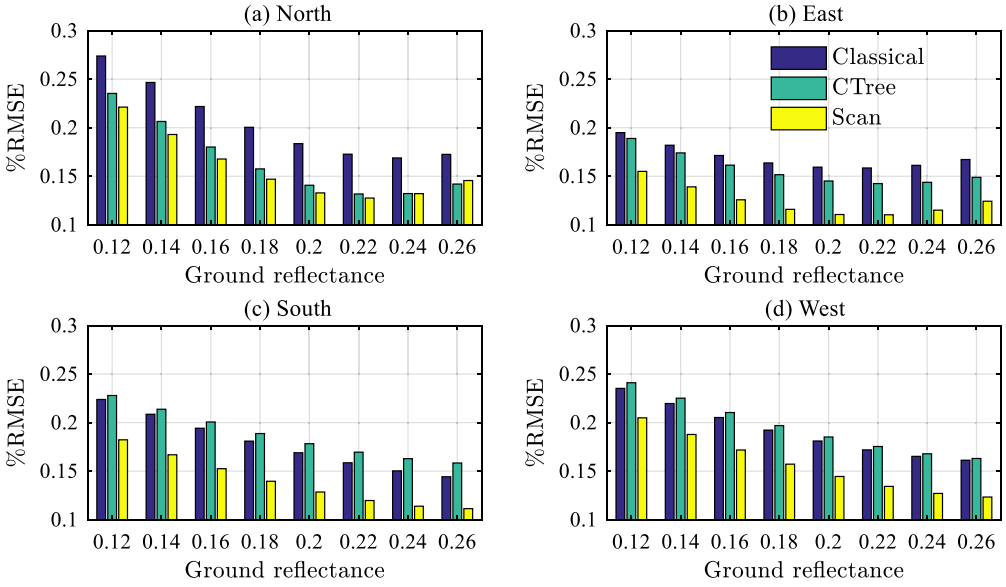

Fig. 9. %RMSE of the illuminance on vertical planes for different r_g settings.

According to Fig. 8, r_g for irradiance should be around 0.16 for its low %RMSE. The %RMSEs of the proposed ISC model were 1.38% to 2.04% lower than the classical model for the north, east, and west-facing vertical pyranometers when the sky condition is determined by the luminance distribution. For south-facing planes, however, the %RMSEs of the two models were comparable, and the difference was 0.24% for the ground reflectance of 0.16. This was probably because of the strong direct irradiance on the south-facing plane. When the sky condition is determined by the CTree, the %RMSEs of the proposed approach were lower than the classical model for the north direction, while were similar for the other directions. This shows the model accuracy relies on the properly determined conditions of the CIE Standard Skies.

Fig. 9 presents the accuracies of the ISC model for the illuminance on the vertically installed lux metre in the four cardinal directions. According to the figure, the r_g of daylight illuminance should be around 0.24 for its low %RMSE, which was higher than that of the full-spectrum radiation. With an r_g of 0.24, the %RMSEs of the proposed ISC model were 4.61% lower than the classical model (Perez et al., 1990) for the vertical illuminance on the east direction, and around 3.6% to 3.8% for the other directions if the sky condition is determined by the luminance distribution. The difference was more significant than the irradiance, probably because the CIE Sky conditions were determined by the luminance instead of the radiance distribution. When the CIE Standard Sky is determined by the CTree, however, the %RMSE of the ISC approach was lower than the classical model in the north and east directions only. The error of the CTree case was probably because the input for the sky identifications was irradiance instead of illuminance. The findings implicate that the proposed ISC model can be more accurate than the classical model for the vertical illuminance and irradiance, as long as the Sky conditions can be correctly identified.

Additionally, Table 4 summarizes the ISC model performance that is evaluated by different error indices, including the RMSE and R^2 with the optimized r_g. The results were in good agreement

Table 4
Performances of the different models, $r_g = 0.16$ for irradiance and 0.24 for illuminance.

Error indices	Approaches	Irradiance				Illuminance			
		N	E	S	W	N	E	S	W
RMSE (W/m^2 and klux)	Classical	17.6	29.8	25.7	29.1	2.26	3.2	3.58	3.58
	CTree	15.6	29.6	26.3	28.8	1.77	2.86	3.88	3.64
	Scanner	15.4	27.0	25.2	26.5	1.77	2.29	2.71	2.75
R^2	Classical	0.893	0.962	0.978	0.968	0.886	0.959	0.962	0.956
	CTree	0.916	0.963	0.977	0.968	0.930	0.967	0.956	0.954
	Scanner	0.918	0.969	0.979	0.973	0.930	0.979	0.978	0.974

with the %RMSE analysis in Figs. 8 and 9. The RMSE in the north direction was 2.3 W/m^2 and 0.51 klux lower than that by the classical model for irradiance and illuminance, respectively. R^2 of the proposed approach suggests the proposed model explained 2.6% and 4.4% more data variations in north direction than the classical model. The CIE Standard Skies, weather determined by the luminance distribution or CTree, give similar R^2 and RMSE for the irradiance and illuminance in the north direction that is determined predominantly by the anisotropic diffuse sky as the focus of the current study.

For other directions, however, the R^2 of irradiance was similar (differences less than 0.005) for all approaches, though the RMSE of the proposed approach (by luminance distribution) was 0.5 to 2.8 W/m^2 higher than the classical one when the CIE Skies were accessible. For illuminance, R^2 of the proposed approach (by luminance distribution) explained 1.7% to 2% more variations than the classical model, and the corresponding RMSEs of the proposed approach were 0.83 to 0.91 klux lower than the classical model. The results suggest multiple error indices should be considered for the error analysis. The performance of the sky conditions determined by CTree, however, was comparable to the classical model, as shown by the differences of R^2 lower than 0.001 for irradiance, and 0.008 for illuminance. The lower accuracies of CTree compared to the luminance distributions were because of the CIE Standard Skies were not accurately identified, which infers the importance of the Sky identification. Nonetheless, the results suggest that the surrogate model interpreted the diffuse luminance and radiance distributions of the CIE Standard Skies as the illuminance and irradiance correctly.

Further to the irradiance and illuminance on vertical planes, the proposed model was validated by the irradiance on the tilt planes, and the accuracy indices were determined by the measurements from February 27 to May 31, 2015. The CIE Standard Skies of the period were determined by the CTree (Lou et al., 2017) since the sky scanner was out of service. The CTree saves the measurement cost, yet leads to a few uncertainties in identifying the Sky conditions. The pyranometers were facing different azimuth directions and in different tilt angles, and the data were recorded and averaged every 10 min. Table 5 specifies the quantity of the accepted data for sensors in different directions, referring to the CIE Guide (CIE, 1994). Less than half of the data were accepted in Level 2 due to the difficulty in measuring E_{HD} by the shadow ring that needs to be adjusted frequently. In addition, a few datasets were removed in Levels 4 and 5, which were different for the measurements in different directions. The r_g was set as 0.16, according to the results of Fig. 9.

Table 6 gives the RMSE, %RMSE, and R^2 of the proposed and the classical (Perez et al., 1990) approaches in estimating the global irradiance on the tilt plane. The RMSEs suggest the proposed approach was more accurate than the classical model for the $\pi/6$-NW (tilt by $\pi/6$, facing northwest), $\pi/4$-S, and $\pi/4$-W, and $\pi/4$-SW directions with a difference of 1.8 to 2.7 W/m^2. The RMSEs of the planes account for 0.5% to 0.6% of the measurement average, and the R^2 results suggest the proposed approach interpreted 0.4% to 0.7% of the data variations. For planes of other tilt angles, the %RMSE differences of the two approaches were lower than 0.3%, and the differences of R^2 were lower than 0.003. Both approaches were more accurate for planes tilted by $\pi/6$ than those tilt by $\pi/3$, which was probably because the irradiance on a low-tilt-plane should be closer to that on the horizontal surface (E_{HG}) as the input. The current CTree gives a rough sky identification using the basic solar radiation measurements. The proposed approach can be more accurate if the CIE Standard Skies are identified more accurately using the more sophisticated data (e.g., vertical irradiance or illuminance).

4. Conclusion

An approach was proposed to surrogate the numerical integration of the luminance and radiance under the 15 CIE Standard Skies for the irradiance and illuminance on tilt planes. The inclined sky component (ISC) was defined as the ratio of the diffuse irradiance or illuminance on tilt planes to that on an unobstructed horizontal plane under the same sky radiance and luminance distributions. This study correlates the ISC of numerical integrations to variables including the type of the CIE Standard Skies, χ_{ref}, α_S, and the plane tilt angle β by the neural network for a fast evaluation of the irradiance and illuminance on tilt PV panels and building envelopes. Validations by the 10-minute data show that the %RMSE of the proposed approach was 1.38% to 2.04% lower than a classical model for irradiance, and 3.6% to 4.6% lower for illuminance on the vertical planes facing most of the four cardinal directions. For planes tilted by $\pi/3$ (60°), $\pi/4$ (45°), and $\pi/6$ (30°), the RMSEs of the proposed model were 1.8 to 2.7 W/m^2 lower than the classical approach in several directions and were comparable for the others. The results suggest that the proposed model was reliable in evaluating the irradiance and illuminance on tilt planes ($< \pi/2$), which is essential for solar energy and daylighting studies.

A major limitation of the work is that the accuracy of the model relies on the appropriate identification of the CIE Standard Skies. The Sky conditions identified by routine measurements of weather stations would lead to extra errors compared to the Skies that are identified by the comprehensive luminance scan. The needs of accurate Sky identifications can lead to burdens in data measurements, and the approaches by routine horizontal measurements should be developed further. Additionally, the current study is limited to unobstructed environments only. Since the CIE Standard Skies specify the radiance and luminance in all the sky directions, the future study should evaluate the radiation and daylight potential in environments when the skydome in obstructed by the surrounding environment.

Declaration of competing interest

The authors declare that they have no known competing financial interests or personal relationships that could have appeared to influence the work reported in this paper.

Table 5
Numbers of the accepted measurement samples for the data of the tilt planes (2015).

Tests		Criteria	Irradiance data										
Level 0		$\alpha_S > 0$	7,004										
Level 1		$\alpha_S > 4°$ $E_{HG} > 20$ W/m^2	6,206										
Level 2	2.1	$0 < E_{HG} < E_{HE}$	2,653										
	2.2	$0 < E_{HD} < 0.8E^1_{HE}$											
	2.3	$0 \leq (E_{HG} - E_{HD}) < E^1_{HE}$											
	2.4	$E_{HD} < 1.1E_{HG}$											
		Vertical directions	Vertical irradiance										
			$\pi/6$, NE	$\pi/6$, SE	$\pi/6$, SW	$\pi/6$, NW	$\pi/4$, N	$\pi/4$, E	$\pi/4$, S	$\pi/4$, W	$\pi/3$, NE	$\pi/3$, SE	$\pi/3$, SW
Level 4		$E_{VG} > 20$ W/m^2	2,620	2,589	2,615	2,594	2,634	2,601	2,623	2,609	2,565	2,556	2,589
Level 5		$E_{VD} > 0$ ($r_g = 0.16$)	2,616	2,584	2,605	2,562	2,627	2,598	2,616	2,574	2,524	2,554	2,562

Note 1: The extraterrestrial irradiance and illuminance are determined by the solar constant of 1367 W/m^2.

Table 6
Accuracy indices of the irradiance on planes with different tilt and azimuthal angles.

Error indices	Approaches	$\pi/6$, NE	$\pi/6$, SE	$\pi/6$, SW	$\pi/6$, NW	$\pi/4$, N	$\pi/4$, E	$\pi/4$, S	$\pi/4$, W	$\pi/3$, NE	$\pi/3$, SE	$\pi/3$, SW
RMSE (W/m^2)	Classical	61.7	67.7	67.2	**64.2**	45.8	74.2	**56.2**	**65.4**	61.4	59.2	**58.6**
	CTree	62.4	67.8	67	**61.6**	46.9	73.1	**54**	**62.7**	61.4	58.6	**56.8**
%RMSE (%)	Classical	13.8	13.9	13.3	**14.8**	12.5	17.8	**13.1**	**15.6**	20.3	16.4	**15.5**
	CTree	14	13.9	13.3	**14.2**	12.8	17.5	**12.6**	**15**	20.4	16.2	**15**
R^2	Classical	0.942	0.944	0.942	**0.915**	0.934	0.931	**0.939**	**0.934**	0.91	0.938	**0.935**
	CTree	0.94	0.944	0.942	**0.922**	0.931	0.933	**0.944**	**0.939**	0.91	0.939	**0.939**

Table A.1
The weight and bias of the artificial neural network estimating the ISC.

Hidden neuron	$w_{i,1}$ (Sky)	$w_{i,2}$ (χ_{ref})	$w_{i,3}$ (α_S)	$w_{i,4}$ (β)	b_i	w'_i	b'
Neuron 1	−1.545	1.232	0.274	−0.112	3.544	−11.562	−4.453
Neuron 2	0.867	0.938	−0.177	−0.875	−3.711	7.617	
Neuron 3	1	1.635	−0.218	−0.919	−3.957	−2.147	
Neuron 4	0.094	−0.546	−0.093	−0.637	0.454	0.702	
Neuron 5	−0.681	0.588	0.172	0.154	2.01	19.357	
Neuron 6	−2.911	−0.231	−0.035	−0.092	1.686	−5.52	
Neuron 7	−4.998	−0.327	−0.046	−0.148	4.098	5.997	
Neuron 8	5.875	0.337	0.039	0.167	−4.867	4.341	
Neuron 9	0.848	−0.947	−0.173	−0.212	−1.714	5.144	
Neuron 10	9.435	−1.291	−0.199	−0.539	0.097	0.49	
Neuron 11	−0.348	1.723	−0.051	0.527	0.805	−1.497	
Neuron 12	10.067	−1.446	−0.239	−0.678	−0.086	−0.425	
Neuron 13	−3.252	−0.306	−0.055	−0.107	1.626	3.821	
Neuron 14	−0.036	1.127	−0.022	0.176	0.529	−5.265	
Neuron 15	0.089	−1.199	0.041	−0.282	−0.558	−7.287	
Neuron 16	0.217	0.712	1.482	−0.161	1.474	−2.796	
Neuron 17	−0.326	1.86	−0.124	0.681	−0.097	−0.474	
Neuron 18	0.252	0.719	1.485	−0.142	1.507	2.748	
Neuron 19	9.671	1.154	0.271	0.3	1.392	−0.084	
Neuron 20	0.035	−0.166	0.284	−0.712	0.987	−2.4	
Neuron 21	−0.102	0.006	−0.287	0.664	−1.007	−2.707	
Neuron 22	1.439	−1.553	−0.077	0.331	−3.637	−6.347	

CRediT authorship contribution statement

Siwei Lou: Methodology, Software, Validation, Formal analysis, Data curation, Writing - original draft, Writing - review & editing, Visualization, Funding acquisition. **Danny H.W. Li:** Conceptualization, Resources, Supervision, Project administration. **Dawei Xia:** Investigation, Resources, Funding acquisition. **Isaac Y.F. Lun:** Formal analysis, Writing - review & editing. **Wenqiang Chen:** Investigation, Visualization. **Yanping Yang:** Resources.

Funding

The work was conducted under the following projects:

1. *A Fundamental Study of Anisotropic Sky Radiance and its Effect on Building Envelopes in City Environments* (in Chinese: 天空散射辐射的各向异性规律及对城市建筑表面辐照度作用的基础研究), supported by the National Natural Science Foundation of China (ID: 51808139).

2. *Research on the renovation of facade about the existing residential building in Lingnan area based on energy track* (in Chinese: 基于用能轨迹的岭南地区既有住宅立面更新研究) supported by the National Natural Science Foundation of China (ID: 51708137)

Appendix

See Table A.1.

References

Alshaibani, K., 2011. Finding frequency distributions of CIE standard general skies from sky illuminance or irradiance. Light. Res. Technol. 43 (4), 487–495.

Ben Othman, A., Belkilani, K., Besbes, M., 2018. Global solar radiation on tilted surfaces in Tunisia: Measurement, estimation and gained energy assessments. Energy Rep. 4, 101–109.
Bournas, I., Dubois, M.-C., 2019. Daylight regulation compliance of existing multi-family apartment blocks in sweden. Build. Environ. 150, 254–265.
Chen, W., Li, D.H.W., Lou, S., 2019. Estimation of irregular obstructed vertical sky components under various CIE skies. Energy Procedia 158, 309–314.
Chi, D.A., Moreno, D., Navarro, J., 2018. Correlating daylight availability metric with lighting, heating and cooling energy consumptions. Build. Environ. 132, 170–180.
CIE, 1994. Guide to Recommended Practice of Daylight Measurement. CIE Central Bureau, Vienna, Austria.
CIE/ISO, 2003. Spatial Distribution of Daylight - CIE StandArd General Sky. CIE Central Bureau, Vienna, Austria.
Costanzo, V., Evola, G., Marletta, L., Pistone Nascone, F., 2018. Application of climate based daylight modelling to the refurbishment of a school building in sicily. Sustainability 10 (8), 2653.
Dahmani, K., Dizene, R., Notton, G., Paoli, C., Voyant, C., Nivet, M.L., 2014. Estimation of 5-min time-step data of tilted solar global irradiation using ANN (Artificial Neural Network) model. Energy 70, 374–381.
Darula, S., Kittler, R., Gueymard, C.A., 2005. Reference luminous solar constant and solar luminance for illuminance calculations. Sol. Energy 79 (5), 559–565.
Fan, J., Wu, L., Zhang, F., Cai, H., Ma, X., Bai, H., 2019. Evaluation and development of empirical models for estimating daily and monthly mean daily diffuse horizontal solar radiation for different climatic regions of China. Renew. Sustain. Energy Rev. 105, 168–186.
Ghazali, A., Salleh, E.I., Haw, L.C., Mat, S., Sopian, K., 2017. Performance and financial evaluation of various photovoltaic vertical facades on high-rise building in Malaysia. Energy Build. 134, 306–318.
Kim, C.-H., Kim, K.-S., 2019. Development of sky luminance and daylight illuminance prediction methods for lighting energy saving in office buildings. Energies 12 (4), 592.
Kittler, R., Darula, S., 2016. Scattered sunlight determining sky luminance patterns. Renew. Sustain. Energy Rev. 62, 575–584.
Lee, H.M., Yoon, J.H., Kim, S.C., Shin, U.C., 2017. Operational power performance of south-facing vertical BIPV window system applied in office building. Sol. Energy 145, 66–77.
Li, D.H.W., Chau, N.T.C., Wan, K.K.W., 2013. Predicting daylight illuminance and solar irradiance on vertical surfaces based on classified standard skies. Energy 53, 252–258.
Li, D.H.W., Chau, T.C., Wan, K.K.W., 2014. A review of the CIE general sky classification approaches. Renew. Sustain. Energy Rev. 31, 563–574.
Li, D.H.W., Cheung, K.L., Tang, H.L., Cheng, C.C.K., 2011. Identifying CIE standard skies using vertical sky component. J. Atmos. Sol.-Terr. Phys. 73 (13), 1861–1867.
Li, D.H.W., Li, C., Lou, S.W., Tsang, E.K.W., Lam, J.C., 2015. Analysis of vertical sky components under various CIE standard general skies. Indoor Built Environ. 25 (4), 703–711.
Li, D.H.W., Lou, S., 2018. Review of solar irradiance and daylight illuminance modeling and sky classification. Renew. Energy 126, 445–453.
Li, D.H.W., Lou, S., Lam, J.C., Wu, R.H.T., 2016. Determining solar irradiance on inclined planes from classified CIE (international commission on illumination) standard skies. Energy 101, 462–470.
Li, X., Wei, Y., Zhang, J., Jin, P., 2019a. Design and analysis of an active daylight harvesting system for building. Renew. Energy 139, 670–678.
Li, Z., Xing, H., Augenbroe, G., 2019b. Criterion based selection of sky diffuse radiation models. Sustainable Cities Soc. 50, 101692.
Liu, B.Y.H., Jordan, R.C., 1963. The long-term average performance of flat-plate solar-energy collectors: With design data for the U.S., its outlying possessions and Canada. Sol. Energy 7 (2), 53–74.
Lou, S., Chen, W., Li, H.W.D., Wang, M., Chen, H., Lun, Y.F.I., Xia, D., 2019a. Tilted photovoltaic energy outputs in outdoor environments. Sustainability 11 (21).
Lou, S., Li, D.H.W., Chen, W., 2019b. Identifying overcast, partly cloudy and clear skies by illuminance fluctuations. Renew. Energy 138, 198–211.
Lou, S., Li, D.H.W., Lam, J.C., 2017. CIE standard sky classification by accessible climatic indices. Renew. Energy 113, 347–356.
Lou, S., Li, D.H.W., Lam, J.C., Chan, W.W.H., 2016. Prediction of diffuse solar irradiance using machine learning and multivariable regression. Appl. Energy 181, 367–374.
Luo, T., Yan, D., Lin, R., Zhao, J., 2014. Sky-luminance distribution in beijing. Light. Res. Technol. 47 (3), 349–359.
Luo, Y., Zhang, L., Liu, Z., Wu, J., Zhang, Y., Wu, Z., 2018. Numerical evaluation on energy saving potential of a solar photovoltaic thermoelectric radiant wall system in cooling dominant climates. Energy 142, 384–399.
Mangione, A., Mattoni, B., Bisegna, F., Iatauro, D., Zinzi, M., 2018. On the validity of daylight factor for evaluating the energy performance of building. In: 2018 IEEE International Conference on Environment and Electrical Engineering and 2018 IEEE Industrial and Commercial Power Systems Europe. EEEIC/I & CPS Europe. pp. 1–4.
Moon, P., Spencer, D.E., 1942. Illumination from a non-uniform sky. Illum. Eng. 37, 707–726.
Ng, E., Cheng, V., Gadi, A., Mu, J., Lee, M., Gadi, A., 2007. Defining standard skies for Hong Kong. Build. Environ. 42 (2), 866–876.
Notton, G., Paoli, C., Vasileva, S., Nivet, M.L., Canaletti, J.-L., Cristofari, C., 2012. Estimation of hourly global solar irradiation on tilted planes from horizontal one using artificial neural networks. Energy 39 (1), 166–179.
Perez, R., Ineichen, P., Seals, R., Michalsky, J., Stewart, R., 1990. Modeling daylight availability and irradiance components from direct and global irradiance. Sol. Energy 44 (5), 271–289.
Robledo, L., Soler, A., 2001. On the luminous efficacy of diffuse solar radiation. Energy Convers. Manage. 42 (10), 1181–1190.
Robledo, L., Soler, A., 2003. Modeling the luminous efficacy of diffuse solar radiation on inclined surfaces for all sky conditions. Energy Convers. Manage. 44 (1), 177–189.
Shishegar, N., Boubekri, M., 2017. Quantifying electrical energy savings in offices through installing daylight responsive control systems in hot climates. Energy Build. 153, 87–98.
Suárez-García, A., Granados-López, D., González-Peña, D., Díez-Mediavilla, M., Alonso-Tristán, C., 2018. Seasonal caracterization of CIE standard sky types above burgos, northwestern Spain. Sol. Energy 169, 24–33.
Sudan, M., Mistrick, R.G., Tiwari, G.N., 2017. Climate-based daylight modeling (CBDM) for an atrium: An experimentally validated novel daylight performance. Sol. Energy 158, 559–571.
Sudan, M., Tiwari, G.N., 2016. Daylighting and energy performance of a building for composite climate: An experimental study. Alex. Eng. J. 55 (4), 3091–3100.
Sudan, M., Tiwari, G.N., Al-Helal, I.M., 2015. A daylight factor model under clear sky conditions for building: An experimental validation. Sol. Energy 115, 379–389.
Tian, Z., Perers, B., Furbo, S., Fan, J., Deng, J., Dragsted, J., 2018. A Comprehensive Approach for Modelling Horizontal Diffuse Radiation. In: Direct Normal Irradiance and Total Tilted Solar Radiation Based on Global Radiation under Danish Climate Conditions, vol. 11, (5), p. 1315.
Tregenza, P.R., 1980. The daylight factor and actual illuminance ratios. Light. Res. Technol. 12 (2), 64–68.
Tregenza, P.R., 2004. Analysing sky luminance scans to obtain frequency distributions of CIE standard general skies. Light. Res. Technol. 36 (4), 271–279.
Tregenza, P.R., Waters, I.M., 1983. Daylight coefficients. Light. Res. Technol. 15 (2), 65–71.
Wittkopf, S.K., Soon, L.K., 2007. Analysing sky luminance scans and predicting frequent sky patterns in Singapore. Light. Res. Technol. 39 (1), 31–51.
Yun, S.-I., Kim, K.-S., 2018. Sky luminance measurements using CCD Camera and comparisons with Calculation models for predicting indoor illuminance. Sustainability 10 (5), 1556.